



UNIUNEA EUROPEANĂ



GUVERNUL ROMÂNIEI  
MINISTERUL MUNCII, FAMILIEI,  
PROTECȚIEI SOCIALE ȘI  
PERSONELOR ÎN VÂRSTĂ  
AMPOSDRU



Fondul Social European  
POS DRU 2007-2013



Instrumente Structurale  
2007-2013



MINISTERUL  
EDUCAȚIEI  
NAȚIONALE  
OPOSDRU



UNIVERSITATEA  
„ALEXANDRU IOAN CUZA”  
din IAȘI



„Alexandru Ioan Cuza” University, Iași

The Faculty of Physics

# The study of thin films of doped zinc oxide deposited by sequential laser ablation

Ph D candidate

Tudor Bogdan Coman

Research advisor

Prof. Dr. Ovidiu Florin Călțun

Iași, september 2013

# **1. The current status of research regarding zinc oxide with applications in optoelectronics and spintronics**

## **1.1 Doped zinc oxide: general properties and current uses**

ZnO is a II-VI semiconductor. It is stable in a compact hexagonal crystalline structure of the wurtzite type, where each ion is surrounded by four opposite ions placed in a tetrahedral configuration. The lattice constants are  $a = 3.25 \text{ \AA}$  and  $c = 5.2 \text{ \AA}$ . It has a wide band gap of 3.4 eV, making it useful for applications using light in the ultraviolet domain. It has intrinsic n type conductivity.

It is currently used especially for sensors, collar cells and various other optoelectronic devices. In thin film form it is transparent, being used for electrodes insensitive to light from the visible spectrum. Because the elementary cell lacks an inversion centre, it has piezoelectric properties that can be taken advantage of when building transducers. Similar to other semiconducting oxides like  $\text{TiO}_2$  [1] it is also a material suitable for making gas sensors, being sensitive to the presence of a number of organic as well as inorganic compounds.

Regarding doping of ZnO with the intent of changing some of its characteristics, there are two main directions. For increasing the carrier density, Al and Ga are often used. Electron concentrations of over  $10^{20} \text{ cm}^{-3}$  and resistivities of about  $10^{-4} \Omega\text{-cm}$  are obtained. For the purpose of controlling the band gap and attaining different values suitable for applications, alloys are made with oxides of Mg, Be (increase) and Cd (decrease).

## **1.2 Zinc oxide doped with aluminium: a transparent electrode**

Doping zinc oxide with donor impurities is done with the purpose of improving its electrical properties. Among all the usable dopants, aluminium is enjoying special attention, ZnO:Al having been thoroughly investigated during the past years. The applications for this material are in electronics and optoelectronics, most often in the form of transparent conducting electrodes. ZnO is cheap, abundant, easy to obtain and non toxic. In addition, the low resistivities that can be obtained for ZnO make it the most promising material to replace indium tin oxide, the current material of choice in industry [2].

AZO is investigated in thin film form, two of the most frequently used deposition methods being magnetron sputtering [2] and pulsed laser ablation, or PLD. It is desirable to obtain films with thicknesses of tens of nanometres, on large surfaces and for low substrate temperatures (maximum  $200^\circ\text{C}$ ).

Studies on the variation of the resistivity with the Al percentage in ZnO seem to indicate an optimum value of 2% [4]. Resistivities of about  $10^{-4}$   $\Omega$ -cm, which are considered necessary for applications, have been obtained for thin films deposited by PLD [5, 6], but at high temperatures. Park et al. [6] optimized the process and found that the optimum temperature is 300°C. Gong [5] noticed a minimum of the resistivity at 360°C.

Although zinc oxide is transparent over the whole visible spectrum, Al doping can lead in some situations to an improvement of the transmittance [7]. Instead, a decrease in the near IR region can be seen [5, 7]. The band gap of AZO is larger than that of undoped ZnO, but the magnitude of the increase depends on the experimental conditions used and can be anywhere from  $\approx 0.05$  eV to  $\approx 0.7$  eV.

Research regarding this material is still going on. Several problems concerning the uniform distribution of resistivity and the atmospheric stability [2] are still to be solved. Room temperature deposition on different types of substrates can be further improved by optimizing the experimental process in regard to various deposition parameters.

### **1.3 An introduction to diluted magnetic semiconductors (DMS)**

Diluted magnetic semiconductors are obtained by doping non-ferromagnetic semiconductors with low concentrations of magnetic ions. As a result of doping, the new material becomes ferromagnetic. DMS are interesting as potential materials for future spintronics applications. MacDonald et al. [8], talking about DMS, propose that the materials meet the following requirements:

- FM induced by a preferably low dopant concentration
- Curie temperatures of over 500 K
- Magnetic properties that are independent of the random distribution of the dopant ions in the material
- Intense magneto-optic effects, for writing/reading the magnetically memorized information

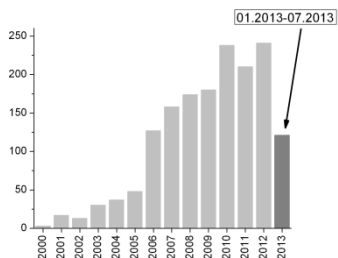
### **1.4 ZnO as DMS: substrates, methods of synthesis, dopants used**

The idea of using ZnO for obtaining diluted magnetic semiconductors took shape after some theoretical results were published [9]. For over a decade, manganese was one of the most used dopants. Alongside Mn, Co was also used often, but tests have been made with all other 3d elements, from Sc to Cu. The number of papers using Fe or Cu is larger than that investigating Sc or Ti. Co-doping has been employed in order to inject additional free carriers and to

stabilize or enhance the ferromagnetism. N and some alkali metals (mostly Li, sometimes Na or K) have been used with the intention of obtaining a DMS based on p-ZnO.

Most of the research focused on ZnO in thin film form. The materials were polycrystalline, but in some situations authors worked with single crystals. Regarding the deposition process, for epitaxial growth we can note a preference for sapphire ( $\text{Al}_2\text{O}_3$ ) substrates. Other substrates used were Si and even ZnO, while from the amorphous ones glass and quartz were chosen. The preparation methods were diverse, not only for obtaining zinc oxide and adding the dopant, but also for deposition of the films. Some of the most common technologies include pulsed laser deposition, magnetron sputtering and chemical methods (mainly sol-gel).

The yearly number of articles dedicated to investigating the magnetic properties of zinc oxide has risen almost constantly during the past decade. For constructing an overall picture of the evolution of the DMS domain, we used the articles from the Thomson Reuters database ([www.isiknowledge.com](http://www.isiknowledge.com)), which we filtered based on the inclusion in the title of the keywords “ZnO” and “magnet\*” or “ZnO” and “ferromagnet\*”. An approximate evolution of the number of papers published can be seen in figure 1.1.



---

Figure 1.1 The evolution of the number of articles on the subject of the ferromagnetism of ZnO between 2000 – 2013 (july)

---

## 1.5 Approaches and results specific to the field of ZnO-based DMS

Some of the first articles dedicated to ZnO have investigated several dopants simultaneously, with the purpose of identifying the promising ones. In general, we can remark that the resulting properties are dependent not only on the preparation method, but also on the parameters used. Ueda [10] investigated the existence of ferromagnetic properties for the semiconductor doped with some of the transition metals: Co, Cr, Ni, Mn. For the thin films containing CO, he

showed the FM of the samples by measuring a hysteresis loop, and the maximum  $T_c$  was almost 300 K. Also, it has been experimentally proven that  $T_c$  and  $M_s$  depend on the carrier concentration. Mn, Cr and Ni did not lead to a FM behaviour of the material.

Venkatesan et al. [11] used all of the TM, with a fixed concentration of 5%. At ambient temperature the measurements revealed values of  $1.9 \mu_B/\text{Co}$  at saturation, close to the 1.8 obtained by Ueda. Instead Cr, Mn or Cu, when added to ZnO, did not make it ferromagnetic. Fukumura et al. [12] produced a large number of samples (9 impurities x 9 concentrations). Measurements indicated the lack of FM for all dopants, all the way down to 3 K.

In the past few years, elements from other regions of the periodic table have been used more and more frequently. A look over the published works reveals that Mn and Co still are the dopants of choice, although metals like Fe, Cu or Ni are starting to be used more often. There are also some attempts to dope ZnO with rare earths. There is also an increase of the percentage of articles dealing with the ferromagnetism of zinc oxide as a nanostructured material: nanoparticles, nanowires, nanocolumns, nanotubes etc.

Even if there is no consensus over the experimental process that could lead to reproducible results, there are a few exceptions. Kittilstved et al. [13] claim the possibility of manipulating the ferromagnetism of ZnO doped with Co or Mn, while in [14] the authors reach the conclusion that the ferromagnetic properties of zinc oxide deposited on r-sapphire substrates, under different experimental conditions, can be reproduced.

In experiments, the dependence of the saturation magnetization on the electron concentration in ZnO doped with Mn has been highlighted in papers like the one belonging to Yang et al. [15]. The authors established for the investigated samples that  $M_s$  varies almost linearly with  $n_e$ , with a maximum of  $5 \mu_B/\text{Mn}$  for concentrations of  $1.2 \times 10^{20} \text{ cm}^{-3}$ . On the other hand Kittilstved [13], also for films doped with Mn, reaches the conclusion that the magnetic characteristics are influenced by the hole concentration, in agreement with the predictions of Dietl [9]. When the dopant is Co, the charge carriers responsible for the FM are the electrons.

From all the aspects regarding the magnetism of zinc oxide it is worth mentioning the emergence of ferromagnetism in the undoped oxide. The phenomenon is interesting because it would allow a much simpler transition of ZnO towards a MS by avoiding the introduction of foreign ions in the lattice. This direction of ZnO research is independent, including its own theoretical and experimental papers, but the material is not a true DMS as defined previously.

Current theories assume that the observed FM is closely related to the presence of structural defects in the material, mainly point defects. In [14], the authors identify zinc vacancies as the cause of FM, using as support for their conclusions a series of ab-initio calculations. The saturation magnetization increased with increasing defect concentration, but decreased for values larger than a critical value. The explanation of this assumes that the magnetic moments annihilate each other when, due to a high density, pairs of defects couple antiferromagnetically. Chen et al. [16] demonstrate the role of defects in stabilizing the ferromagnetism at room temperature by observing a deterioration of the FM following heat treatments in an O<sub>2</sub> environment, where a reduction of the number of oxygen vacancies takes place.

From the theoretical papers for which the conclusions could be verified in practice we mention the one belonging to Sluiter et al. [17]. The conclusion reached by the authors is that doping with both holes as well as electrons would promote the ferromagnetism in ZnO doped with Mn or Co, and in order to verify this hypothesis they chose as an acceptor dopant Li. The results of measurements made at room temperature confirmed that the supplementary addition of Li to (Zn, CO)O leads to an increase of the saturation magnetization, the effect being proportional to the Li content, for a constant Co percentage.

## 1.6 Particularities of the ferromagnetism in ZnO

The diluted magnetic semiconductors can be characterized by several quantities: saturation magnetization, coercive field, remanence. Summarizing a series of results, the typical values of the magnetic field for which saturation is reached are around 0.1-0.2 T, while the coercive field is at most 2-300 Oe. At saturation, the magnetic moment per dopant ion varies from 0.01 to 6  $\mu_B$ , some of the values being close to the maximum theoretical ones (especially for Co). The obtained materials always showed anisotropy of the magnetization. Usually, measurements could be performed along one of the crystal axis, for which the direction was known following epitaxial growth. Some films have an easy axis, while others display perpendicular anisotropy.

The formation of secondary phases is an unwanted effect. When the dopant concentration is higher than the solubility limit in the host semiconductor, the excess dopant can segregate at grain boundaries or it may form clusters or compounds, in combination with the elements of the host matrix. Since the majority of impurities used are transition metals, the formation of clusters (in the case of Fe, Ni and CO, the ferromagnetic elements) could be responsible for the overall ferromagnetic behaviour of the sample.

Usually, phase composition analysis is done by X-ray diffraction. The fact that no peaks other than those belonging to zinc oxide are present in the XRD patterns is not necessarily evidence that those phases are not present in the material. Taking into account that most of the times the samples contain low dopant concentrations (dopant ions relative to total metallic ions), it is possible that the eventual parasite phases formed are below the detection limit of the method.

Contamination of the samples can happen in other ways. Since their volume is small and the magnetic moments to be measured are also small, it is imperative to identify and eliminate other sources of signals, no matter how small. For example, the transfer of metal in small quantities can be achieved when handling the substrate with a tweezers [18], especially if the substrate is abrasive (like  $\text{Al}_2\text{O}_3$  is).

## **1.7 The current status of research regarding the ferromagnetism of Ni-doped ZnO**

ZnO:Ni was and is studied under different forms including powders, nanoparticles, nanostructures and thin films. The paragraphs below will present results from the literature, on this last type of structure.

In general Ni has a lower solubility in ZnO than Mn or Co. In the study of Jin et al. [19], the values for which we still have Ni-Zn substitution are 4-5 % for PLD. More recently, in a series of papers using fast atom beam sputtering, Pandey et al. [20,21] managed to reach 12%. In both cases, when the solubility limit characteristic for each method was surpassed, a secondary phase of NiO was formed, and it could be detected by means of XRD.

Investigating Ni:ZnO with different percentages of Ni, Pandey [20] observes a depreciation of the optical properties once Ni is introduced into ZnO. In addition,  $n_e$  suffers a decrease as a result of doping. The lower values of  $n_e$  were attributed to the annihilation of oxygen vacancies and demonstrated by analyzing the XPS data. In [21], samples obtained by the same group, using the same method and with an identical Ni content, showed ferromagnetic properties this time, although an increase of  $n_e$  of three orders of magnitude compared to the first case and no NiO phase in the XRD patterns seem to suggest an increased sensibility of the final properties to the experimental conditions.

FM in ZnO:Ni has several characteristics in common with other ZnO-based DMS. Summarizing a series of results [21-24] one can note that the saturation magnetization tends to decrease with temperature for a constant Ni

concentration, and for different concentrations but at a fixed temperature in depends on the Ni content in the film. The coercive field values are between 10-300 Oe, while the magnetic moment per dopant ion, given in Bohr magnetons, is 0.2-0.3. Hou et al. [25] obtained (magnetron sputtering)  $0.43 \mu_B/\text{Ni}$  at room temperature for an optimum Ni concentration of 4%, and this value is comparable to the one initially measured by Venkatesan for PLD films with 5% Ni.  $0.49 \mu_B/\text{Ni}$  is reported by Jin et al. [26] for ZnO:Ni deposited on sapphire, although when the substrate is Si (100) this value decreases to  $0.2 \mu_B/\text{Ni}$ .

Curie temperatures of over 300 K are obtained frequently, but are not guaranteed. In 2008, Pivin et al. [23] produced samples that were ferromagnetic at 5 K but paramagnetic at 300 K. The same paper highlights that the characteristics depend on the substrate type.

It is worth mentioning the importance of the oxygen pressure during deposition. In [24], by varying the Ar/O<sub>2</sub> ratio, the authors noticed an increase of the saturation magnetization as the atmosphere became oxygen deficient. The results resemble the ones in [14] for ZnO:Co. The explanation takes into account the increase of the number of oxygen vacancies, confirmed by photoluminescence measurements. The vacancies determine the rise of ferromagnetic ordering, according to a model proposed by Coey [26].

In the future, the study of ZnO still leaves room for progress. Although the  $M_s$  values are of one order of magnitude lower than those of ZnO:Co, Ni remains one of the most promising and most utilized dopants from the transition metal group. The abundance of the experimental results is comparable to that included in the literature dedicated to Co and Mn. From the papers published in the past few years only about half focus on thin films. The others approach so-called modern subject, like nanoparticles and nanostructured materials, ensuring that research in the field of ZnO:Ni follows the current tendencies.

## **2. Experimental techniques used for the deposition and characterization of thin films of ZnO**

### **2.1 The deposition of thin films by laser ablation**

#### **2.1.1 Description of the method and the experimental setup**

Pulsed laser deposition (PLD) is a technique used for the deposition of thin films, which has become frequently used nowadays [27]. It uses a laser beam which interacts, in short bursts, with a solid target. If the energy of the incident pulse is higher than a threshold value characteristic of each substance, the result is a local heating and evaporation (ablation) of the irradiated material. A plasma will form, containing species like atoms, ions and maybe molecules. The plasma will expand perpendicular to the target and will transfer material onto a suitably placed substrate.

The PLD method became very popular due to its versatility. Laser with different wavelengths and pulse durations of nanoseconds or femtoseconds can be used. PLD allows us to deposit elements, compounds and even polymers. There is also the possibility of creating new materials by utilizing two targets or by choosing a deposition atmosphere that influences the final composition of the films. PLD offers a great degree of freedom regarding thin film deposition, this advantage being the main reason of choosing it as a method to work with.

The experimental installation that we have used can be considered a typical one. The laser was excimer type, with Kr-F, with a wavelength of 248 nm and a pulse duration of 90 ns. The number of pulses per second and the energy of each pulse can be varied, depending on the requirements, between 1 and 50 and up to 700 mJ, respectively. The fluence can be set by changing the energy of the pulses or, alternatively, by modifying the spot area on the target by altering the position of the focusing lens. The laser radiation is incident on the target at an angle of 45° and the resulting plasma will expand towards a substrate placed parallel to the target. The substrate holder is fitted with an electric heater, allowing depositions at temperatures up to 900°C.

The target is mounted on an automated carrousel that can accommodate up to six targets, for deposition of films with different compositions. The parameters that can be adjusted are numerous: fluence, pulse frequency, the pressure and composition of the gas in the deposition chamber, the substrate temperature and the distance between the target and the substrate.

### 2.1.2 Types of targets used for the deposition of zinc oxide

The fact that there are several types of targets that can be used opens up the possibility of obtaining different results using the same set of experimental parameters. For the deposition of metal oxides we have two options: metals or oxides. In literature one can notice an obvious bias towards oxide targets, not necessarily for obtaining ZnO, on which we will not insist, but especially for obtaining ZnO doped with various metals.

Although composition of the type  $Zn_{1-x}D_xO$  can be ordered from specialized companies, authors usually prepare the targets themselves. The process consists of several well established steps. The materials (oxides) are initially in powder form, they are mixed in predetermined proportions and the resulting mixture is pressed into a pellet and sintered at high temperatures.

A second solution implies the use of metallic targets. One of the choices is the creation of Zn-D alloys. Another one is based on the creation, in the laboratory, of a mosaic target by adding on the surface of the zinc patches of dopant foil with different shapes and in different positions. A third option is to construct a compound target, half zinc and half another material.

Oxide targets are several times more expensive than metal targets of identical size. In addition, the dopant concentration in the thin film tends to be lower than in the target because there is a difference between the ablation rates of the ZnO and dopant oxide in the composition. Metals, on the other hand, can be used even as thin foil (0.25 mm), further reducing the costs. Mosaic type metal targets, however, also suffer from the differential ablation of the two metals.

### 2.1.3 The sequential ablation method

There is a third option for depositing thin films of doped zinc oxide, and that is to use multiple targets. In the simplest case there are two targets, one of them supplying the zinc and the second one acting as a source of dopant atoms. The method is known in literature as sequential laser ablation. This name describes an algorithm according to which a thin film is formed by alternating depositions from the two targets. The number of papers in which sequential ablation is used is relatively low, no matter the investigated material. Even so, SA is versatile. Watanabe et al. synthesized the compound  $YBa_2Cu_3O_7$  from individual metal targets [28]. In [29], the authors added Si to  $MgB_2$  using  $MgB_2$  and Si targets, and in [30] SA was used to introduce Ni in carbon not only for doping, but also for the creation of alloys.

When it comes to zinc oxide, the examples are few. Misra et al. [31] obtained CdZnO alloys starting from CdO and ZnO. Das [32] doped ZnO with Si

and showed, after XPS data analysis, that the dopant had substituted the Zn in the lattice as  $\text{Si}^{3+}$ . The same group doped ZNO with Al [33] in low concentrations (<1%).

In general, in order to deposit doped ZnO we can use as targets practically any of the combinations oxide/oxide, oxide/metal or metal/metal. The choice of materials is free, any of the proposed combinations being usable. A thin film is obtained by repeating a large number of times a base sequence consisting of the alternating ablation of the two targets. The amount of material deposited per sequence is generally very small, so as to avoid the formation of a multilayer structure. Varying parameters such as pressure, fluence etc. we can deposit by laser ablation monoatomic layers or even sub-monolayers.

Sequential ablation offers the possibility of fine tuning the dopant concentration by changing the ratio of pulses sent on each of the targets. Another advantage is that we can create, starting with two basic materials, any combination (mixture) between them or, in a reactive atmosphere (oxygen), synthesize oxides or oxide alloys. In addition, using metals we can deposit films with a composition identical to that of the layers obtained through the ablation of a single  $\text{ZnO}/\text{D}_2\text{O}_y$  target, but at a reduced cost.

For our research we chose the sequential laser ablation method because it is rarely used for obtaining doped zinc oxide. An initial study was conducted on a simple system, ZnO:Al, and part of the results were used as a starting point for the investigation of ZnO co-doped with Ni and Al.

## **2.2 Investigation methods employed**

We can divide the measurements made on magnetic semiconductors in two main categories, depending on their purpose. The first objective is to investigate the dopant-zinc substitution and the lack of supplementary phases. The second class includes the magnetic measurements, with the main priority being the confirmation of the ferromagnetism. In a third category we could include the determination of properties that are important when we speak about semiconductors in general (optical, electrical and so on). This class of properties tends to be of secondary importance since the materials in question are very rarely intended to be used in applications other than those typical of a DMS.

Various experimental techniques can be used to carry out these investigations, in some situations several alternatives being available. Often, the data acquired supplies more than one type of useful information. In the following paragraphs we will describe some of the techniques that we have used and the way in which this experimental data provides us with relevant information regarding a DMS.

### 2.2.1 Analysis of the structure and composition of the material; ways of verifying that the substitution took place

X-ray diffraction is used in order to gather information regarding the crystalline structure of the material. Usually we record the intensity- $2\theta$  curve, in a  $\theta$ - $2\theta$  experimental configuration. The main things that we can find out are the type of structure (crystalline/amorphous) and the phases in the composition of the material. In the field of DMS, XRD is used mainly as a tool for detecting secondary phases, since the presence of such phases can have a strong influence on the material properties. Any sign of a non-ZnO phase, like oxides of the dopant D or binary oxides of the dopant with zinc, means that the material is no longer a diluted magnetic semiconductor, but a multi-phase compound. Secondary phases present in very small quantities may remain undetected and that is why the results obtained through XRD need to be checked by using complementary techniques.

From the XRD data we can try to check if the substitution dopant/zinc has taken place. Among the noticeable effects is the shift of the diffraction peaks to new values of the  $2\theta$  angle when the dopant is added. This is equivalent with a change of the interplanar distance, and one of the causes is the modification of the bond lengths due to the different atomic radii of the zinc and dopant ions. XRD also allows us to find out the solubility limit of a dopant in ZnO [34].

X-ray photoelectron spectroscopy, a technique used for surface characterization, is another method that can help us investigate the composition of the thin films, this time by identifying the chemical elements in the composition. Although XPS is adequately sensitive and precise, we rarely find that the Zn:O ratio is 1:1, as one would expect in undoped zinc oxide. Instead, large deviations may appear [35], so there is the possibility that the dopant percentages determined by XPS are affected by this and will be far from the actual values. By XPS we can also find out the thickness of a film by detecting the emergence of the peaks characteristic to the elements in the substrate, after we have etched the deposited ZnO.

The position of a maximum in a XPS spectrum can tell us if, for example, the dopant D is surrounded by other atoms of the same type or, by contrary, oxygen atoms. XPS is also useful for detecting intrinsic defects. If there is an asymmetric O 1s peak and we perform a deconvolution there will be two or even three components, one of them corresponding to  $V_O$  [36].

Optical techniques may serve as an additional method of verifying the substitutional doping or of studying the point defects in the material. As a consequence of doping, the transmission spectra may sometimes display

absorption bands that correspond to transition involving energy levels that can be linked to the dopant. For example, d-d transitions characteristic of  $\text{Co}^{2+}$  in tetrahedral coordination were noticed by Tay [37] and considered proof of Co substitution.

A second set of spectroscopic measurements consist of photoluminescence spectra. PL is very useful in the study of intrinsic defects, the presence of these in the material giving rise to energy levels in the forbidden band. PL detects only radiative recombinations (transitions).

### 2.2.2 Magnetic measurements

When we speak of a DMS we are mainly interested to obtain ferromagnetic properties. Their presence is necessary in order to classify the material as a DMS, but often it is not enough. For this reason the magnetic measurements become of primary importance. In many articles, the part dedicated to the FM of DMS materials is approached by simply measuring the magnetization-field curves, with the intention of highlighting the existence of a hysteresis cycle. If we only want to confirm the FM character of the sample following the doping of ZnO, this is the minimum that we need to use when it comes to magnetic measurements, and in literature there is a considerable number of papers of this kind.

The existence of a hysteresis cycle is proof of the FM in the material, but it does not offer details about the source of the signal. We have at least two components, one due to the substrate and one of the film itself. Talking about the ferromagnetism of the film this can be intrinsic to the DMS, due to secondary phases like metal clusters or both, and we need additional data to discern between them.

$M_s$  is the most relevant quantity that we can use to characterize the magnetic properties of the samples. It serves as an indicator of the degree to which the spins introduced by the dopant in the lattice are aligned. Determining the Curie temperature can be useful sometimes, but the presence of FM at ambient temperature is considered enough.

## Conclusions

We described the pulsed laser ablation method of depositing thin films and tried to emphasize some of its advantages. As for the measurements, we tried to divide them in several categories, depending on what we are trying to find out regarding the investigated compound. We presented some of the

techniques that we have used, trying to select from the information that they offer that which is important for a DMS.

We deposited ZnO:Al (AZO) from two metal targets, with two objectives in mind. The first was the calibration of the method in order to easily predict the dopant concentration in the future. The second was the investigation of the way in which Al is integrated in the ZnO lattice, and for this purpose a series of structural (XRD), compositional (XPS) and optical measurements were employed. We also measured the electrical properties, AZO being a well known transparent electrode.

### 3. The deposition and characterization of thin films of ZnO doped with Al deposited by sequential laser ablation using two targets

#### Introduction

In the first sub-chapter are presented the results pertaining to the variation of the structural and optical properties as a function of the oxygen pressure in the deposition chamber. For the second sub-chapter we obtained and investigated thin films with different concentrations of aluminium, at a fixed pressure. The following parameters were kept constant: the substrate temperature (300 K), the target to substrate distance (5 cm) and the pulse frequency (5 Hz). The fluence was fixed by choosing the energy of the incident pulse to be 205 mJ and the focusing lens was placed at 46 cm from the target.

#### 3.1 The study of the influence of the pressure on the properties of thin films of ZnO:Al deposited by sequential laser ablation

In our experiment it is necessary to use oxygen. In order to determine the pressure most suited for deposition of AZO using sequential ablation from metal targets we chose a fixed ratio of pulses per sequence (30 on Zn and 15 on Al). We used glass substrates that were degreased, rinsed with acetone and ethanol, cleaned in an ultrasound bath for 10 minutes and dried by blowing nitrogen on them. In order to deposit a film we used a number of 287 sequences, for a cumulative total of 8910 pulses on the zinc target and 4455 pulses on the Al target.

In literature, zinc oxide and AZO are deposited by laser ablation at oxygen pressures ranging from  $10^{-5}$  mbar to 1 mbar. We obtained a set of samples using the pressures given in table 2.1, covering a wide range of values. We focused on the structural and optical properties and based on these qualities we chose the pressure to be used for the deposition of other samples of doped or co-doped zinc oxide.

Sample	P1	P2	P3	P4	P5	P6	P7	P8	P9
Pressure (mbar)	$5 \times 10^{-4}$	$5 \times 10^{-3}$	$1 \times 10^{-2}$	$3 \times 10^{-2}$	$5 \times 10^{-2}$	$7 \times 10^{-2}$	$1 \times 10^{-1}$	$5 \times 10^{-1}$	3

Table 2.1. The oxygen pressures used for the deposition of thin films of AZO with a fixed aluminium concentration, at room temperature

### 3.1.1 Structural properties

The structural analysis was performed by X-ray diffraction with a Shimadzu 6000 using the Cu  $k_\alpha$  radiation ( $\lambda = 1.5406 \text{ \AA}$ ). The diffraction patterns reveal that the crystalline structure changes its type depending on the pressure used during the deposition. At low values (P1, P2, P3) there is a dominant peak corresponding to the reflection on the (110) family of planes belonging to ZnO. The shift from the normal value of  $2\vartheta = 56,53^\circ$  (reference chart JCPDS 086254 for ZnO) can be caused by the mechanical tensions present in the crystal lattice, which are most likely caused by the oxygen vacancies or zinc interstitials present as a result of the low oxygen pressure used.

The thicknesses for P3-P7 decrease gradually from 353 to 125 nm. This is equivalent to an increase of the deposition rate. The increase of the (110) peak amplitude with decreasing pressure can be linked to the layer thickness, a study belonging to Liang [38] showing a similar behaviour for the (110) peak. On the other hand, the mean free path of the particles in the ablation plasma is larger at low pressures, and the species that reach the substrate will have energies that are high enough to rearrange themselves, leading to an improvement of the crystalline quality of the film. This effect can be noticed for ZnO deposited by other means, for example HIPIMS [3].

The position of the (110) peak makes it difficult to assign it correctly since metallic zinc has the (102) reflection at  $2\vartheta = 54,32^\circ$ . In addition, we can see that the amplitude decreases with increasing pressure, a behaviour which supports the idea of incomplete oxidation of zinc in an oxygen deficient atmosphere. The peak is symmetrical therefore it belongs to only one of these two phases. P4 and P5 also have a maximum around  $2\vartheta = 56^\circ$ , but its position approaches that of ZnO (110) with increasing pressure. The existence of ZnO (100) and ZnO (101) in the XRD patterns of samples P1-P3 confirms the formation of the oxide even at the lowest pressures used. For these reasons, we can exclude any metallic presence in the samples.

The other samples in the series (P5-P9) have a polycrystalline structure with low amplitude diffraction peaks. Above  $3 \times 10^{-2}$  mbar the increase of the pressure does not have any significant changes in the XRD patterns.

Analyzing the surface of the films by atomic force microscopy we can identify a change of morphology when the pressure increases from 1 to  $3 \times 10^{-2}$  mbar, as it can be seen in figure 3.4. At low pressure (P3) the 2D images show a

number of isolated peculiarities of approximately identical sizes (50 nm) that are distributed evenly across the entire surface. The 3D image shows that these are cone-like structures. They are also present on P4, with the main difference that they are more densely packed and cover the film surface continuously. For this reason, the average roughness decreases from 6.6 nm (P3) to 5.5 nm (P4). At higher pressures there are no significant changes of the morphology and the roughness continues to decrease.

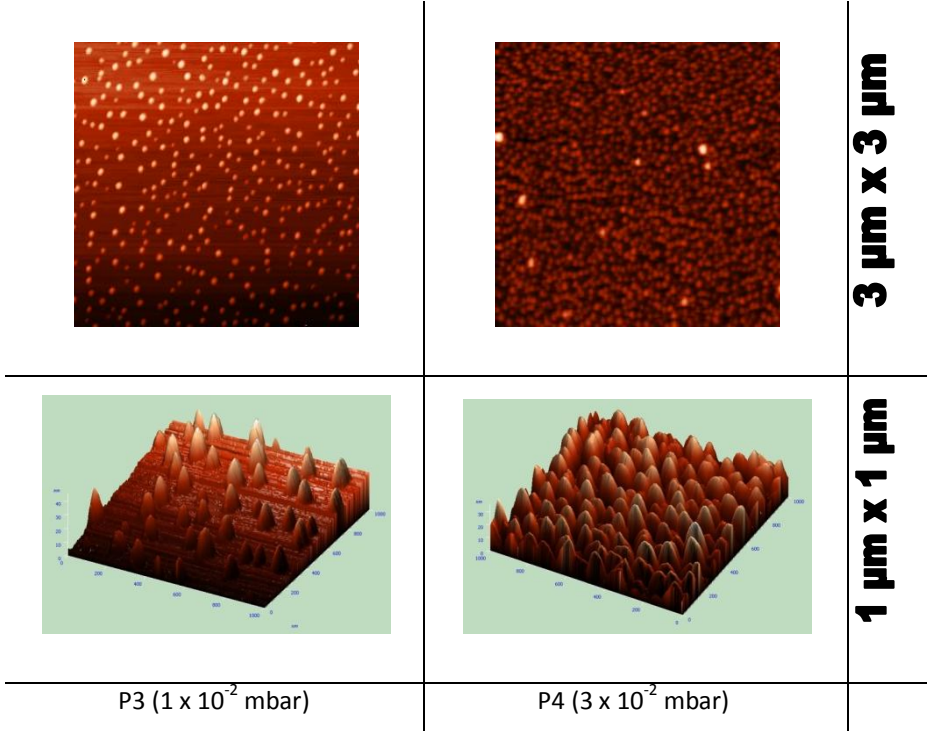


Figure 3.4 The influence of the oxygen pressure on the morphology of the AZO films; the change of the way in which the surface is organized takes place at an intermediary pressure, between the values used for depositing the two samples shown above

### 3.1.2 Optical properties

We investigated the optical properties of the thin films by recording the photoluminescence spectra (Perkin Elmer LS 55 fluorescence spectrophotometer)

and transmission spectra (Evolution 300, Thermo Scientific). The samples obtained at the extremes of the pressure interval used in our study had very low values of the transmittance. This is the case for P1, P2, P8 and P9. The dark colour of AZO deposited at low pressures is attributed to a deviation from stoichiometry which leads to an excess of zinc, most likely as interstitials that absorb the incident light [39].

Starting with the pressure of  $1 \times 10^{-2}$  mbar, the  $T(\lambda)$  spectra take the shape that we expect for ZnO. The curves of samples P4-P7 are almost identical, with average values of T of over 80 % between 400 and 1100 nm. The values of T for P3 reach a maximum of only 80% and in a short interval, and for wavelengths from the infrared region there is a decrease of the transmission. This behaviour is caused by the presence of Al in the sample.

Regarding the photoluminescence spectra, data acquired for P1 and P2 show no emission. For films deposited at pressures between  $1 \times 10^{-2}$  mbar (P3) and  $1 \times 10^{-1}$  mbar (P7) we have a signal which maintains its aspect but changes its amplitude. The lowest values are those for P3 and P7, and the most intense PL signal is the one of sample P5, deposited at  $5 \times 10^{-2}$  mbar.

Based on the information collected so far we could conclude that the interval between  $1 - 10^{-2}$  mbar is adequate for the deposition of ZnO:Al using our method and the experimental parameters that we have chosen. Some problems like the concentration of oxygen defects, the existence of mechanical tensions or the issue of the film adherence to the substrate are minimized. With the exception of sample P3, all the other ones have similar characteristics. For these reason, the oxygen pressure was fixed at  $5 \times 10^{-2}$  mbar for all subsequent depositions.

### **3.2 Deposition and characterization of thin films of ZnO:Al with a variable concentration of Al**

After choosing the pressure we studied the properties of samples with varying dopant concentration. This time, the pressure was kept at  $5 \times 10^{-2}$  mbar. In order to change the aluminium content in the films we kept the number of pulses on the Zn target at 30 per sequence and the number of pulses of Al was varied between 3 and 15 (see table 3.2). As a reference we used an undoped ZnO film (ZO) deposited using the same conditions, for a total number of 10000 pulses on Zn.

Sample	C1	C2	C3	C4	C5
--------	----	----	----	----	----

Pulses Zn/Al	30/3	30/6	30/9	30/12	30/15
Table 3.2. The composition of the base sequences used for depositing ZnO thin films with different percentages of aluminium					

### 3.2.1 Analysis of the structure and composition of the thin films

All the peaks detected by XRD can be attributed to ZnO and there are no traces of secondary phases. In the pattern of the ZO sample we can see only the reflections corresponding to the (002) and (004) families of planes, which means that the majority of the crystallites are oriented with the c axis perpendicular to the substrate. For the TF with low aluminium content (C1, C2, C3) the preferential orientation is preserved, but the amplitude of the (002) maximum decreases as the number of pulses on the Al target increases (figure 3.7). There is also a shift of the peak position. Computing the values of the lattice constant c we can note that they increase gradually with the dopant concentration. In the case of C1-C5, for which there is a continuous variation of the dopant concentration, the most likely cause is the presence of aluminium interstitials [38], evidence that not all Al ions substitute Zn in lattice nodes.

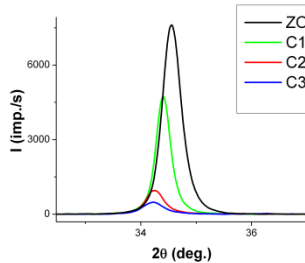


Figure 3.7. The XRD patterns for samples C1-C3 and for the reference sample ZO, showing the presence of the typical hexagonal ZnO structure, with a preferential orientation along the c axis

We used the XPS technique (Axis Nova, Kratos Analytical) for determining the Al concentration of the samples. The percentage was expressed as the ratio Al/(Al+Zn). As it can be seen in figure 3.10, for a constant value of 30 pulses on the Zn target there is a linear dependence between the number of pulses on the Al target and the Al concentration in the film. This result confirms that we can control the dopant distribution through the number of pulses shot on the dopant target.

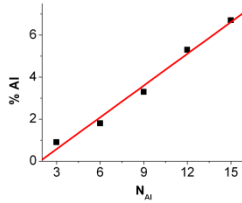
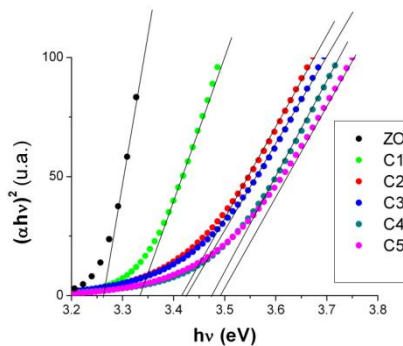


Figure 3.10. The dependence of the dopant concentration on the number of pulses sent on the Al target during a sequence

We conducted a depth study to show that the structure resulted is not a multilayer. The deviations of the Al percentage from the average value are small. There are no significant changes and no periodic variations, meaning that the dopant was uniformly spread in the host semiconductor.

### 3.2.2 Optical and photoluminescence properties

The thin films have average transmittance values of 90% (450-1000 nm), independent on the aluminium concentration, There is also a progressive shift towards lower wavelengths of the fundamental absorption band. After computing the optical band gap we can confirm that  $E_g$  increases with increasing Al concentration, as it can be seen in figure 3.12 where the values corresponding to each sample are given by the intersection of the linear fit with the abscissa. The results are in agreement with the expectations regarding the way in which the BG varies in ZnO doped with Al. For samples similar to our own, in which it was assumed that Al is also present as interstitials, Park et al. [40] noticed modifications within a narrow interval, from 3.34 to 3.38 eV, for  $Al_2O_3$  between 1 and 3 % in the target used.



---

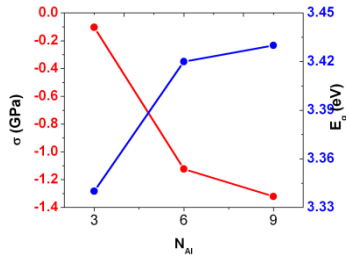
Figure 3.12. Linear fitting of the  $(\alpha hv)^2=f(hv)$  plots for determining the optical band gap

---

The increase of  $E_g$  could be caused by the stress in the film. In our case the stress is of intrinsic origin, being caused by the structural defects in the material. In order to compute the stress values for the samples C1-C3, for which we only have the (002) maximum in the diffraction patterns, we used the following formula [41] for the stress in the plane parallel to the film surface:

$$\sigma = -233 \frac{c_{film} - c_0}{c_0} \text{ GPa}$$

, where  $c_0 = 5.2066 \text{ \AA}$  is the lattice constant of bulk ZnO (single crystal, stress-free). We can see in figure 3.13 that the values of  $\sigma$  decrease while the BG increases with increasing Al content. Sharma [42] attributed the decrease of  $\sigma$  on the tendency of Al to occupy interstitial positions. In our case, the continuous decrease of the stress indicates a progressive increase of the number of Al interstitials in samples from the C series, while the negative values are indicating that the stress is of compressive origin [38].




---

Figure 3.13 The change of the stress and band gap values with changing Al concentration (samples C1 – C3)

---

We recorded the photoluminescence spectra at room temperature using an excitation wavelength of 325 nm, for which the PL signal detected had maximum intensity. The general shape of the curves suggests that the signal is made up of several components. In order to identify each emission band we performed a deconvolution using Lorentz profiles.

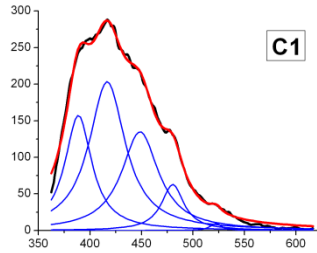


Figure 3.14. The photoluminescence spectrum of the sample C1, with the five components

At approximately 395 nm is the band corresponding to the exciton recombinations in ZnO (electron from CB with hole from VB). The other bands are the result of radiative transitions that imply at least one energy level associated with an intrinsic defect. The green emission centered on 520 nm (2.38 eV) is associated in literature with the presence of antisite  $O_{Zn}$  defects [43]. Based on the calculations of Lin et al. [44],  $Zn_i$  has a level which is 2.9 eV above the VB, and the transition  $Zn_i$ -VB generates photons with a wavelength of  $\approx 426$  nm. Zeng et al. [45] identified several components of the blue emission, including one at 440 nm and another one at 488 nm, and those transitions involved energy levels induced in the forbidden band by the presence of  $Zn_i$ . In order to explain the emission at wavelengths higher than 426 nm (in our case at 453 nm), Zeng assumes the existence of additional levels in the vicinity of the main  $Zn_i$  level. The 485 nm band is a result of the transition between the energy levels of  $Zn_i$  and  $V_{Zn}$ .

### 3.2.3 Electrical properties

We used the in line four point probe method [41]. Injecting the current  $I$  through the outer probes, measuring the voltage  $V$  between the inner probes and applying the correction for samples of finite thickness, the resistivity is:

$$\rho = \frac{\pi}{\ln 2} d \frac{V}{I}$$

$d$  is the thickness of the thin film, which we determined from surface profilometry measurements. The resistivities were of the order of  $10^{-1} \Omega \cdot \text{cm}$ , showing an improvement of four orders of magnitude over the undoped sample, which had  $\rho_{ZnO} = 6.8 \times 10^3 \Omega \cdot \text{cm}$ . The results are comparable to other results reported relatively recently [38].

C1-C5 have resistivities that increase in order. One explanation for this could be the one proposed by Venkatachalam [47], who also noticed a continuous increase of  $\rho$  with dopant concentration and attributed it to a deterioration of the

crystallinity. On the other hand, for our method the optimum Al concentration for which  $\rho$  has a minimum may be lower than the lowest concentration included in our study.

For an n type semiconductor, the case of ZnO and AZO, the resistivity is [46]:

$$\rho = \frac{1}{ne\mu}$$

$e$  is the elementary charge,  $n$  is the electron concentration and  $\mu$  is the mobility. Mobility varies by no more than one order of magnitude when we change the dopant content [48], so the decrease of the resistivity from  $10^3 \Omega \cdot \text{cm}$  for ZO (0% Al) to  $\approx 10^{-1} \Omega \cdot \text{cm}$  (AZO) can be attributed mainly to an increase of  $n$ . Thus, we can conclude that a fraction of the Al ions substitute zinc in lattice nodes and act as donors.

## Conclusions

Optimization of the process regarding the pressure showed that an interval between  $3 \times 10^{-2}$  mbar and  $1 \times 10^{-1}$  mbar is suitable for obtaining AZO with good optical properties. For the samples with different aluminium concentrations the XPS analysis confirmed that there is a linear dependence between the number of pulses on the dopant target and the Al percentage in the thin film. This information can be used in order to deposit films with known compositions.

From XRD we find that some of the Al ions occupy interstitial positions instead of substituting the zinc in lattice nodes. The PL spectra show that there is a considerable concentration of  $\text{Zn}_i$  in undoped ZnO, meaning that the experimental method itself favours the formation of this type of defect. Conductivity measurements reveal an improvement of  $\rho$  with doping, which is a sign that Al substitution was only partially realized. The weak dependence of  $\rho$  on the concentration can also be attributed to the tendency of Al to end up as interstitials.

## 4. Magnetic properties of the thin films of ZnO co-doped with Ni and Al deposited by sequential laser ablation using three targets

### Introduction

In this chapter we shall present the results concerning the synthesis and characterization of zinc oxide doped with two elements. The chosen combination is Ni & Al, which is supposed to accomplish two things: the introduction of magnetic ions in the lattice (Ni) and the generation of additional free carriers (Al). We intended to check the following:

- The influence of a varying Al concentration for a constant percentage of Ni in ZnO;
- The influence of a varying Ni concentration for a constant percentage of Al in ZnO;
- The influence of Al when compared with samples of ZnO:Ni.

We maintained constant the substrate temperature (295 K) and the oxygen pressure ( $5 \times 10^{-2}$  mbar). In order to obtain thin films with different concentrations of Al or Ni we repeated for approximately 300 times a sequence with the structure (30 pulses Zn/ N pulses N/ n pulses Al). We created individual series for which we kept constant the number of pulses for one of the dopants and we changed the number of pulses on the second dopant target, with the purpose of investigating the role of each additional element.

Sample characterization focused on their magnetic properties since these are of interest when introducing Ni into ZnO. The techniques that offer other types of information were considered to have a complementary role. As a reference, thin film of ZnO:Ni were deposited also by sequential laser ablation.

### 4.1 Structural and magnetic properties of the system $\text{Zn}_{0,99-x}\text{Ni}_x\text{Al}_{0,01}\text{O}$

The thin films of ZnO co-doped with Ni and Al were obtained using a base sequence of the type:

$$(30 \text{ pulses Zn} / 3 \text{ pulses Al} / N \text{ pulses Ni})$$

The number of pulses on the Ni target, N, was varied between 5 and 15, while the number of pulses on the Al target was constant and equal to three. The samples that we used as a reference were deposited using the same values for N, but with n = 0.

Using XRD we could not detect secondary phases for any of the compositions in our study. The films have a preferred orientation along the c axis which they keep even after increasing the number of pulses on the Ni target. We used the XPS technique to determine the Ni concentrations and the oxidation states in which this element is present in ZnO. Since in all the cases the last deposition was made from the Ni target, we acquired initial spectra without etching the surface. Ni  $2p_{3/2}$  is situated between 854.5 eV – 856.9 eV while Ni  $2p_{1/2}$  is around 875 eV. The values are far from those corresponding to metallic Ni (870 and 852.2 eV [49]). In addition, the presence of satellite peaks at  $\approx$  863 eV and 882 eV is a sign the Ni is bound to oxygen [21], therefore we can consider that the oxidation of the dopant was complete.

Afterwards we acquired the spectra after etching the surface with Ar ions. In this way information about the oxidation state of Ni in the volume of the sample becomes available. The shape of the signal can be seen in figure 4.4 a. For all the films we notice the emergence of peaks corresponding to metallic Ni ( $Ni^0$ ) at  $\approx$  852 și 869.5 eV. There are also the maxima of  $2p_{1/2}$  (872.5 – 872.7 eV) și  $2p_{3/2}$  (854.6 – 854.8 eV) corresponding to oxidized Ni and we can also see the satellite peaks at  $\approx$  862 and 880 eV. If the positions of the peaks indicate the existence of Ni in the 2+ state, the energy difference between them is about 17.6 – 17.7 eV. This is different from that of  $Ni^{2+}$  in NiO and can be considered proof that Ni substituted the Zn in ZnO [50].

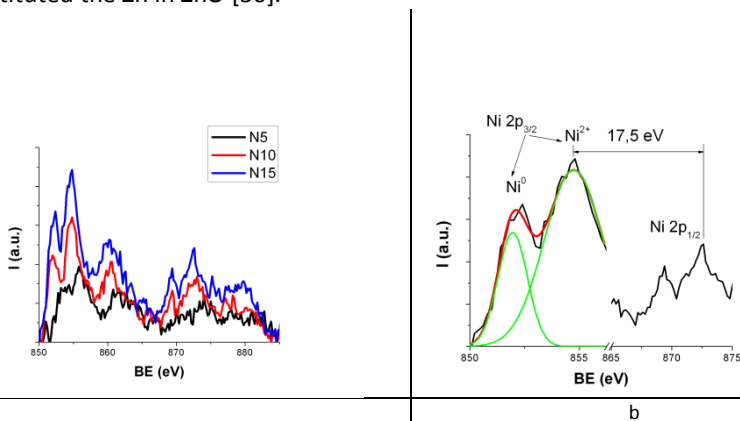


Figure 4.4 a) Ni 2p depth spectra acquired after surface etching with Ar ions; b) Deconvolution of the signal of the N15 thin film, showing the new components

We made an analysis of the XPS spectra of oxygen, for which we performed a deconvolution. At low values (529.3 eV) we have an intense signal

attributed to  $O^{2-}$  in the hexagonal structure of ZnO [51] (in tetrahedral coordination with four zinc ions). At 531 eV there is a peak which is usually associated with  $O^{2-}$  from the oxygen deficient regions in the material. The concentration of  $V_O$  defects in the material may play a role in explaining the magnetism of the films within the bound magnetic polaron model.

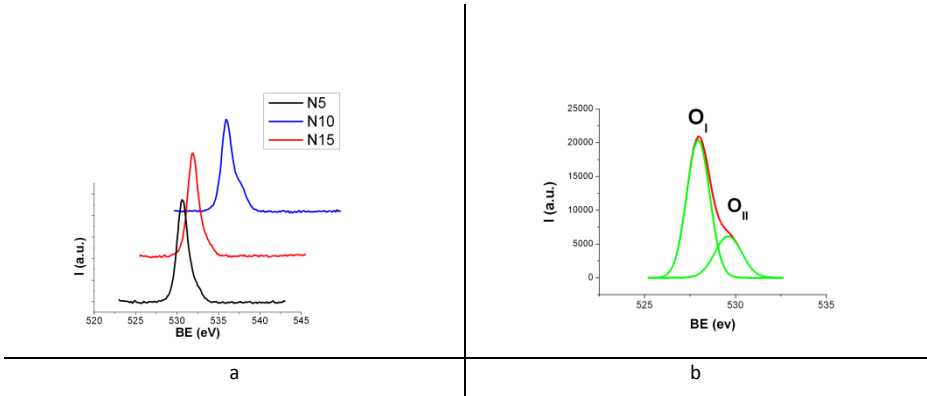


Figure 4.5 a) The asymmetric profile of O 1s for samples in the N series; b) Deconvolution into two components associated with oxygen in ZnO ( $O_I$ ) and oxygen vacancies ( $O_{II}$ )

The Zn/O ratio determined Through XPS is larger than one, indicating a deviation from stoichiometry. Between the number of pulses on Ni (N) and the Ni concentration in the films  $C_{Ni}$  there is a simple dependence of the form:

$$C_{Ni} (\%) = 3 + N$$

From the transmission spectra we can see that the impact of the changing Ni content on the transmittance values is stronger at lower wavelengths. The average values between 400 – 1180 nm are 91% (N = 5), 88% (N = 10) and 80% (N = 15), the most important decrease taking place when the number of Ni pulses per sequence increases from 10 to 15.

The coloration of the samples and the decrease of the transmittance are attributed to light scattering on defects [52], this effect being most obvious for the film with the highest concentration of oxygen vacancies (according to XPS). At wavelengths of over 1180 nm the spectra coincide, with T between 80 and 90% and no tendency to decrease in the IR, as one would expect after doping with Al. Computing the optical band gap we found the values of 3.31, 3.34 and 3.34 eV for N = 5, 10, 15. It seems that the values do not depend on the Ni concentration. For TF of ZnO doped only with Ni, the BG was about 3.23 eV, also independent of N. Adding Al leads to an increase, similar to the case of ZnO:Al. The variation of the

Ni content in the samples is large while the aluminium remains at 1%, meaning that Al has a much stronger influence over the final band gap. Just as in the case of AZO, it is very likely that only a fraction of the Ni ions substitute the zinc, which would explain why  $E_g$  is practically the same when the Ni content varies by 10% from N5 to N15.

The amplitude of the signal in the photoluminescence spectra is inversely proportional to the Ni percentage in ZnO. After deconvolution of the signal we find the same components that were discussed in subchapter 3.2.2. With increasing N there is a general reduction of the intensity of the signal, but the effect is much more pronounced for the maximum corresponding to exciton recombinations. This is equivalent to an increase of the contribution of the signal resulted from the transitions initiated from the  $Zn_i$  level in the forbidden band.

The magnetic properties were investigated using a vibrating sample magnetometer. The magnetic field-magnetization curves were acquired with the field parallel to the thin film surface. To highlight the effect of adding the dopants an undoped ZnO sample was measured first and it turned out to be diamagnetic. As a general fact, all the samples that contained Ni showed ferromagnetic characteristics, the M-H curves for the samples in the series ZnO:Ni and ZnO:(Ni, Al) displaying the saturation phenomenon and the existence of remanent magnetization and coercive field.

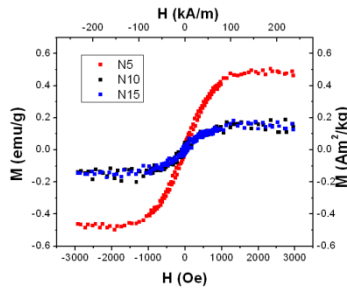


Figure 4.8 The M-H curves for the TF of ZnO:(Ni, Al), recorded at 300 K in the  $H_{||}$  configuration

For a number of 3 pulses of Al per sequence, the hysteresis curves of the samples deposited with 5, 10 and 15 pulses of Ni are showed in figure 4.8. The saturation magnetization is maximum for the thin film with  $N = 5$ , which corresponds to a Ni concentration of 8% (table 4.1). The value is 0.48 emu/g (equivalent to  $0,09 \mu_B/\text{Ni}$ ), but if N is changed then it drops to 0.16 emu/g ( $\approx 0,02 \mu_B/\text{Ni}$  for N10, 13% Ni in ZnO and  $\approx 0,01 \mu_B/\text{Ni}$  for N15, 18% Ni in ZnO). These

values are of the order of magnitude for which other results have been reported in literature for this type of material [21-24].

Compared to the samples doped only with Ni the role of aluminium in improving the magnetic properties is seen only in the case of N5, for which there is an increase of the saturation magnetization of three times compared to the sample with  $n = 0$ . For  $N = 10$  the changes are negligible while  $M_s$  is larger for the sample with  $N = 15$  but 0% Al. There is a positive contribution from the Al only for the smallest Ni content. The ratio of the saturation magnetization of the co-doped (Ni & Al) and the doped (Ni) samples, for identical values of  $N$ , is decreasing as the number of pulses on the Ni target is increased.

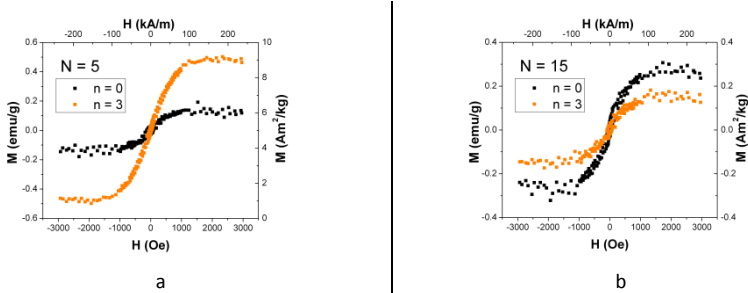


Figure 4.9 The effect of adding Al ( $n$  pulses per sequence) to the composition of ZnO:Ni on the hysteresis cycles

For the ferromagnetism of these samples there are several possible explanations: on one hand, the presence of Ni<sup>0</sup> in the material suggests the likely formation of metallic Ni clusters, an element that is ferromagnetic. On the other hand, from the XPS data we know that Ni is also present in the form Ni<sup>2+</sup>, bound to oxygen and replacing Zn, so the ferromagnetism could be intrinsic. It is possible that there is not only one source for the FM but multiple contributions, each with its own mechanism.

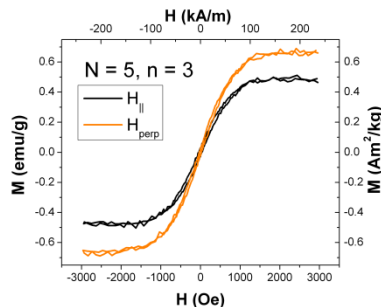


Figure 4.10 Hysteresis curves traced for the field parallel and perpendicular to the film surface, for the samples with N = 5

---

A study of the FM of ZnO:Ni due to nanometric Ni clusters was conducted by Mao et al. [53]. The  $M_s$  value of 0.4 emu/g (approximately 0,21  $\mu_B$ /Ni) are close to those of our films, but the behaviour was different: the magnetization increased linearly with the applied magnetic field and the M-H curves were identical for different field orientation in relation to the sample. In single crystals, nanoclusters formed following the implantation of nickel ions in ZnO were detected by Zhou et al. [54] using XRD. The measurements revealed a superparamagnetic behaviour [55]. Our films doped with Ni and co-doped with Ni and Al, which we deposited by sequential laser ablation, displayed a clear hysteresis and the measurements recorded with the magnetic field perpendicular to the sample surface revealed an anisotropy of the magnetization (figure 4.10).

The presence of a fraction of the Ni ions as  $Ni^{2+}$  replacing Zn in the crystal lattice means that this material also has diluted magnetic semiconductor characteristics. One of the main mechanisms in DMS is that of ferromagnetism mediated by free charge carriers: the spin polarized electrons, aligned after the interaction with a magnetic dopant ion, will travel through the material and will interact with other magnetic ions, realizing in this way the alignment of magnetic moments that are too far apart to interact directly.

Compared to the thin films doped only with Ni, the introduction of Al leads to an increase of the saturation magnetization only for sample N5. We remind here that Al was initially chosen as additional dopant for the specific purpose of supplying charge carriers. The electrical resistance of the co-doped samples deposited by sequential laser ablation are outside of the scale, being at least five orders of magnitude higher than those of the films of ZnO:Al. Usually, substitutional  $Ni^{2+}$  found in ZnO should not alter the electron concentration. However, the addition of Ni may lead, in some cases, to a decrease of the conductivity and a reduction of 2-3 orders of magnitude of the carrier concentration as a result of the annihilation of oxygen vacancies [21]. In chapter 3 we considered that the change of the resistivity is caused mainly by the change of the electron concentration, so following the same logic we can conclude that in our samples the carrier concentration is not large enough to carry out the alignment of distant spins.

This means that another mechanism is at the source of the ferromagnetism in ZnO:(Ni, Al), and it must also be present in ZnO:Ni. In this series  $M_s$  increases when we increase the number of Ni pulses per sequence. As opposed to other methods, the use of sequential laser ablation leads to a particular structure of the thin films. It is reasonable to assume that in the thin

layer formed following the ablation of the Ni target the Ni concentration will be higher than in the adjacent regions, therefore the distances between the Ni ions will be, on average, lower.

The behaviour of the system in this situation is modelled in computational papers using, for example, density functional theory. Sluiter et al. [17] found that for  $\text{Ni}^{2+}$  the parallel alignment is favoured for ions in neighbouring lattice sites. Hernandez et al. [56] found that a stable ferromagnetic state is established for Ni – Ni distances of about 6.2 Å. Due to the order in which the targets are ablated, the substitutional  $\text{Ni}^{2+}$  will be distributed mainly in a plane of atoms. The average distance between Ni ions placed in different lattice nodes will decrease as the Ni content (number of Ni ions) increases. As a consequence, higher values for N will lead to an increase of the probability that  $\text{Ni}^{2+}$  ions will end up closer together favouring their parallel alignment. In this way, a higher fraction from the total number of dopant ions will contribute to the FM of the sample and the saturation magnetization should rise. This reasoning can justify the variation of  $M_s$  with N for the films in the series ZnO:Ni.

Taking into account the presence of oxygen vacancies detected in our samples using XPS, it is possible that another mechanism responsible for the intrinsic FM of DMS might be involved: the FM due to the bound magnetic polarons (BMP) [26]. This model assumes the existence of localized electrons, like those trapped by an oxygen vacancy, that realize the spin polarization of neighbouring magnetic moments. A so-called magnetic polaron will be formed. The polarons that are sufficiently close to one another can interact and in this way a ferromagnetic character can be induced in the whole sample [57]. The BMP model was proposed as an explanation for the FM of ZnO:Ni in the situations when the electron concentrations are low but there is a considerable population of intrinsic defects ( $V_o, \text{Zn}_i$ ) [58].

Assuming the existence of only one of the mechanisms described in the previous paragraphs as the explanation for the FM we note the lack of correlation between the VSM measurements and the data obtained using other investigation techniques. For this reason we can conclude that the ferromagnetism is not necessarily intrinsic to the DMS obtained using our method and it could have multiple sources.

## **4.2 magnetic properties of the system $\text{Zn}_{0,83-\gamma}\text{Ni}_{0,17}\text{Al}_\gamma\text{O}$**

In this section will be presented the results of the investigations concerning the influence of the second dopant, aluminium, on the properties of Zn(Ni, Al)O. This time we tracked the contribution of a varying concentration of Al on the ferromagnetic characteristics. For the deposition of the thin films we

maintained a constant number of pulses of Ni per sequence (15) and we modified the number of pulses of Al (noted with  $n$ ) between 3 and 9.

Although the aluminium concentration increases with the number of pulses on the Al target it remains relatively low, reaching a maximum of 3 % for  $n = 9$ . Even in this situation, the influence of Al on some of the material properties is evident, being much stronger than that of Ni which is present in concentrations that are 5-10 times higher. For example, through XRD we find the same behaviour as for the samples in the series ZnO:Al (chapter 3.2.1): the decrease of the (002) peak intensity, the shift towards lower values of the  $2\theta$  angles and an increase of the full width at half maximum with increasing  $n$ .

Comparing the data with that acquired previously, the increase of the lattice constant  $c$  is a good indicator that the way in which Al enters the crystal lattice of ZnO is independent of the presence of the second dopant. We can say that it has, in this case also, a tendency to occupy interstitial positions.

The XPS spectra of Ni display minor variations of intensity and contain the same peaks that have been discussed in chapter 4.2. The percentage on non-oxidized Ni found in the  $\text{Ni}^0$  state remains unchanged; if we are dealing with Ni clusters, the variations of the ferromagnetic characteristics cannot be attributed to the variation of the Ni content (which is constant) or to the change of the cluster distribution in the material (the same for all the thin films and given by the structure of the base sequence). On the other hand, Al modifies the amplitude of the  $\text{O}_{11}$  component. Al has a much larger affinity for oxygen than zinc and it manages to compensate some of the oxygen vacancies [59] that usually appear in ZnO.

The optical band gap increases from 3.33 eV ( $n = 3$ ) to 3.44 eV ( $n = 9$ ). The values are practically identical to those of ZnO:Al deposited using the same number of pulses of Al per sequence. This is a sign that Ni, although present in the zinc oxide in proportion of 16-18 %, does not contribute significantly to the variation of  $E_g$ . This has been discovered earlier, when we calculated the BG of the TF in which the Ni content was varied. The information obtained now shows that we can control this quantity by means of the Al content and it is enough to introduce small percentages to see the effects.

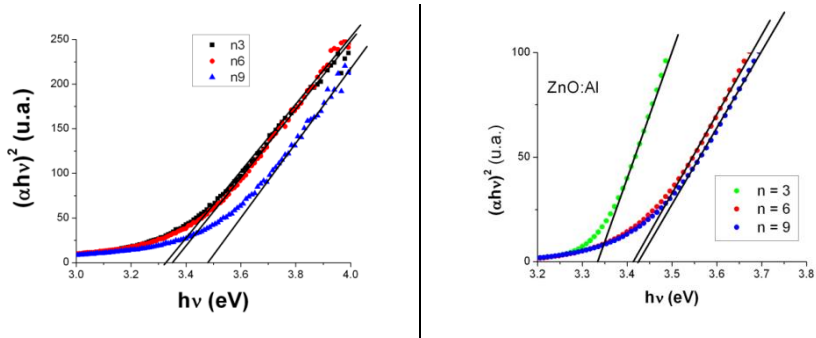


Figure 4.14 The increase of the band gap with the number of pulses of Al for ZnO:(Ni, Al). In the image on the right are shown, for comparison, the BG of the AZO samples deposited with identical values of  $n$  per sequence

The hysteresis loops are shown in figure 4.15. The saturation magnetization is maximum (0.78 emu/g) for a number of Al pulses per sequence and minimum (0.18 emu/g) for  $n = 3$ . The sample labelled n6 has the highest  $M_s$  among the thin films that we have investigated. The variations of this quantity with the Al content are significant, with small increases (one percent) of the concentration of the non-magnetic dopant leading to larger variations of the  $M_s$  than those caused by modifying the magnetic dopant concentration (Ni) with 5 %.

Since there are no changes in the composition of the samples, the same possible sources of the ferromagnetism discussed previously are present in this case. There is no direct correlation between the concentration of Al and  $M_s$ . Taking into account the way in which we noticed the saturation magnetization to vary in the presence/absence of Al (previous sub-chapter) we have enough proof to state that the model of long range ordering mediated by free carriers does not apply for this series of thin films. The magnetic behaviour of the system as a whole will be determined by the sum of individual contributions from different sources. Determining the exact contribution of each source needs further investigation and it is difficult to do because the overall picture is very complex: the thin films have a particular periodic depth structure, there is most likely a secondary phase in the form of Ni clusters in the material, the films have different types of intrinsic defects and so on.

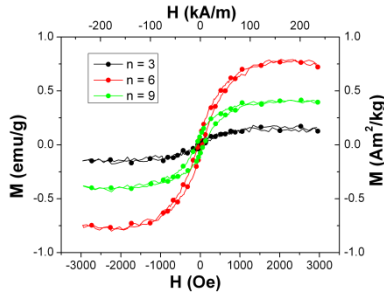


Figure 4.15 Magnetization – field curves for the TF with varying Ni concentration

Although adding Al in various quantities to ZnO doped with Ni has an obvious impact on the saturation magnetization, Al does not play the part for which we initially chose to use it when we decided to investigate this combination of dopants. Instead it acts indirectly on the magnetic properties of the system, most likely by modifying some of the characteristics used to explain the emergence of FM by means of some of the mechanisms described in the previous sub-chapter.

## Conclusions

The main novelty item of this study is the use of the sequential laser deposition technique for depositing  $Zn_{1-x-y}Ni_xAl_yO$  from three metal targets in oxygen atmosphere. The method itself allows a good control of the composition and offers the possibility of controlling the distribution of the dopant in the volume of the film by altering the target ablation sequence and the number of pulses.

The materials have the typical ZnO hexagonal structure with a preferential (002) orientation and no secondary phases detectable by XRD. Although present in much smaller quantities, Al has a stronger effect than Ni on some material properties, like the lattice constant and the band gap.

From the VSM measurements we found out that the samples displayed FM properties. FM is linked to the presence of Ni in ZnO and this was confirmed by tracing the M-H curves for a series of additional thin films of ZnO:Ni. Although there are significant changes of  $M_s$  when modifying the Al content, the free carrier mediated long range magnetic ordering model does not explain this results. The high resistivity of the films, associated with a low electron

concentration, is due to the presence of Ni and no improvement was noticed after co-doping with Al, unlike in the case of ZnO:Al (chapter 3).

Since the XPS data shows that some of the Ni ions are present as substitutional Ni<sup>2+</sup>, a DMS type phase will be present in the thin films. In this case we offered an alternative explanation for the FM, based on the bound magnetic polaron model, which requires the presence of intrinsic defects in the material. In our samples we have oxygen defects (detected by XPS) and zinc interstitials (emission bands in the PL spectra). In the same time, part of the dopant is in the form Ni<sup>0</sup> possibly distributed as Ni cluster of nanometre size. The clusters could contribute to the FM signal of the samples but additional measurements are needed in order to clarify this aspect.

## References

- [1] D.Mardare, N.Iftimie, M.Crișan, M.Răileanu, A.Yildiz, **T.Coman**, K.Pomoni, A. Vomvas, *J Non-Cryst Solids* **357** (2011) 1774–1779
- [2] T.Minami, *Thin Solid Films* **516** (2008), 5822–5828
- [3] V.Tiron, **T.Coman**, L.Sirghi, G.Popa, *J OPTOELECTRON ADV M* **15**(2013), 77 - 81
- [4] Y.Liu, J.Lian, *Appl. Surf.Sci.* **253**(2007), 3727-3730
- [5] L.Gong, Z.Ye, J.Lu, L.Zhu, J.Huang, X.Gu, B.Zhao, *Vacuum* **84** (2010), 947-852
- [6] S.M.Park, T.Ikegami, K.Ebihara, P.K.Shin, *Appl. Surf. Sci.* **253** (2006), 1522–1527
- [7] E.L.Papadopoulou, M.Varada, K.Kouroupis-Agalou, M.Androulidaki, E.Chikoidze, P.Galtier, G.Huyberegts, E.Aperathitis, *Thin Solid Films* **516** (2008), 8141-8145
- [8] A.H.MacDonald, P.Schiffer, N.Samarth, *Nat. Mater.* **4** (2005), 195-202
- [9] T.Dietl, H.Ohno, F.Matsukura, *Phys. Rev. B* **63** (2001)
- [10] K.Ueda, H.Tabata, K.Tawai, *Appl. Phys. Lett.* **79** (2001), 988-990
- [11] M.Venkatesan, C.B.Fitzgerald, J.G.Lunney, J.M.D.Coe, *Phys. Rev. Lett.* **93** (2004), 177206
- [12] Z.W.Jin, T.Fukumura, M.Kawasaki, K.Ando, H.Saito, T.Sekiguchi, Y.Z.Yoo, M.Murakami, Y.Matsumoto, T.Hasegawa, H.Koinuma, *Appl. Phys. Lett.* **78** (2001), 3824-3826
- [13] K.R.Kittilstved, N.S.Norberg, D.R.Gamelin, *Phys. Rev. Lett.* **94** (2005), 147209
- [14] M.Khalid, M.Ziese, A.Setzer, P.Esquinazi, M.Lorenz, H.Hochmuth, M.Grundmann, D.Spemann, T.Butz, G.Brauer, W.Anwand, G.Fischer, W.A.Adeagbo, W.Hergert, A.Ernst, *Phys. Rev. B* **80** (2009), 035331
- [15] Z. Yang, J.L.Liu, M.Biasini, W.P.Beyermann, *Appl. Phys. Lett.* **92** (2008), 042111
- [16] X.G.Chen, Y.B.Yang, R.Wu, R.Liu, X.D.Kong, L.Han, Y.C.Yang, J.B.Yang, *Physica B* **406** (2011) , 1341-1344
- [17] M.H.F.Sluiser, Y.Kawazoe, P.Sharma, A.Inoue, A.R.Raju, C.Rout, U.V.Waghmare, *Phys. Rev. Lett.* **94** (2005), 187204
- [18] M.A.García, E.F.Pinel, J.de la Venta, A.Quesada, V.Bouzas, J.F.Fernandez, J.J.Romero, M.S.Martin-Gonzalez, J.L.Costa-Kramer, *J. Appl. Phys.* **105** (2009), 013925
- [19] Z. Jin, M.Murakami, T.Fukumura, Y.Matsumoto, A.Ohtomo, M.Kawasaki, H.Koinuma, *J. Cryst. Growth* **214** (2000), 55-58
- [20] B.Pandey, S.Ghosh, P.Srivastava, D.Kabiraj, T.Shripati, N.P.Lalla, *Physica E* **41** (2009), 1164–1168
- [21] B.Pandey, S.Ghosh, P.Srivastava, D.K.Avasthi, D.Kabiraj, J.C.Pivin, *J. Magn. Magn. Mater.* **320** (2008), 3347–3351
- [22] K-T.Kim, G-H.Kim, J-C.Woo, C-II Kim, *Surf. Coat. Tech.* **202** (2008,) 5650–5653
- [23] J.C.Pivin, G.Socol, I.Mihailescu, P.Berthet, F.Singh, M.K.Patel, L.Vincent, *Thin Solid Films* **517** (2008), 916–922
- [24] D-L.Hou, R-B.Zhao, Y-Y.Wei, C-M.Zhen, C-F.Pan, G-De Tang, *Curr. Appl. Phys.* **10** (2010), 124–128
- [25] C.Jin, R.Aggarwal, W.Wei, S.Nori, D.Kumar, D.Ponarin, A.I.Smirnov, J.Narayan, R.J.Narayan, *Metall. Mater. Trans. A* **42** (2011), 1-5
- [26] J.M.D.Coe, M.Venkatesan, C.B.Fitzgerald, *Nat. Mater.* **4** (2005), 173
- [27] R.Eason (ed.), *Pulsed Laser Deposition Of Thin Films*, John Wiley & Sons, New Jersey, 2007
- [28] Y.Watanabe, M.Tanamura, H.Asami, Y.Matsumoto, Y.Seki, S.Matsumoto, *PHYSICA C*: **235** (1994), 579-580
- [29] Y.Zhao, M.Ionescu, J.Horvat, A.H.Li, S.X.Dou, *Supercond. Sci. Tech.* **17** (2004), 1247-1252
- [30] N.Sbai-Benchikh, A.Zeinert, H.Caillierez, C.Donnet, *Diam. Relat. Mater.* **18** (2009), 1085-1090
- [31] P.Misra, P.K.Sahoo, P.Tripathi, V.N.Kulkarni, R.V.Nandedkar, L.M.Kukreja, *Appl.Phys.A* **78** (2004), 37-40
- [32] K.Das, P.Misra, L.M.Kukreja, *J. Phys. D: Appl. Phys.* **42** (2009) 165405

- [33] A.K.Das, P.Misra, R.S.Ajimsha, A.Bose, S.C.Joshi, D.M.Phase, L.M.Kukreja, J. Appl. Phys. **12** (2012), 103706
- [34] B.Straumal, B.Baretzky, A.Mazilkin, S.Protasova, A.Myatiev, P.Straumal, J. Eur. Ceram. Soc. **29** (2009), 1963-1970
- [35] S.M.Park, T.Ikegami, K.Ebihara, Jpn. J. Appl. Phys. **45** (2006), 8453–8456
- [36] H.You, J.Yang, J.Y.Zhu, W.F.Xu, X.D.Tang, Appl. Surf. Sci. **258** (2012), 4455–4459
- [37] M.Tay, Y.H.Wu, G.C.Han, Y.B.Chen, X.Q.Pan, S.J.Wang, P.Yang, Y.P.Feng, J. Mater. Sci. – Mater. El. **20** (2009), 60-73
- [38] G.-X.Liang, P.Fan, X.-M.Cai, D.-P.Zhang, Z.-H.Zheng, J. Electron. Mater. **40** (2011), 267-273
- [39] A.V.Singh, M.Kumar, R.M.Mehra, A.Wakahara, A.Yoshida, J.Indian Ins. Sci. **81** (2001), 527-533
- [40] S.H.Park, S.E.Park, J.C.Lee, P.K.Song, J.H.Lee, J. Korean Phys. Soc., **54** (2009), 1344-1347
- [41] R.Hong, H.Qi, J.Huang, H.He, Z.Fan, J.Shao, Thin Solid Films **473** (2005), 58–62
- [42] B.K.Sharma, N.Khare, J. Phys. D: Appl. Phys. **43** (2010), 465402
- [43] Y.Liu, Q.Li, H.Shao, J. Alloy Compd **485** (2009), 529–531
- [44] B.X.Lin, Z.X.Fu, Y.B.Jia, Appl. Phys. Lett. **79** (2001), 943
- [45] H.Zeng, G.Duan, Y.Li, S.Yang, X.Xu, W.Cai, Adv. Funct. Mater. **20** (2010), 561–572
- [46] G.G.Rusu, C.Baban, M.Rusu, *Materiale și dispozitive semiconductoare*, Ed. Univ. „Al.I.Cuza”, Iași, 2002
- [47] S.Venkatachalam, Y.Iida, Y.Kanno, Superlattice Microst. **44** (2008), 127–135
- [48] Y.Liu, J.Lian, Appl. Surf.Sci. **253**(2007), 3727-3730
- [49] <http://srdata.nist.gov/xps/>
- [50] D.L.Hou, R.B.Zhao, Y.Y.Weï, C.M.Zhen, C.F.Pan, G.D.Tang, Curr. Appl. Phys. **10** (2010), 124–128
- [51] P.C.Yao, S.T.Hang, M.J.Wu, W.T.Hsiao, Thin Solid Films **520** (2012), 2846–2854
- [52] T.Tsuji, M.Hirohashi, Appl. Surf. Sci. **157** (2000), 47-51
- [53] X.Mao, W.Zhong, Y.Du, J. Magn. Magn. Mater. **320** (2008), 1102–1105
- [54] S.Zhou, K.Potzger, Q.Xu, G.Talut, M.Lorenz, W.Skorupa, M.Helm, J.Fassbender, M.Grundmann, H.Schmidt, Vacuum **83** (2009), S13–S19
- [55] S.Zhou, K.Potzger, J.von Borany, R.Groetzschel, W.Skorupa, M.Helm, J.Fassbender, Phys. Rev. B **77** (2008), 035209
- [56] R.G.Hernandez, W.L.Perez, M.J.A.Rodriguez, J. Magn. Magn. Mater. **321** (2009), 2547–2549
- [57] H.Morkoc, U.Ozgur, *Zinc Oxide. Fundamentals, Materials and Device Technology*, Wiley VCH Weinheim, 2009, cap. 5.7 p. 311
- [58] S.Yilmaz, E.McGlynn, E. Bacaksiz, J.Cullen, R.K.Chellappan, Chem. Phys. Lett. **525–526** (2012), 72–76
- [59] J.H.Noh, I.S.Cho, S.Lee, C.M.Cho, H.S.Han, J.S.An, C.H.Kwak, J.Y.Kim, H.S.Jung, J.K.Lee, K.S.Hong, Phys. Status Solidi A **206** (2009) 2133–2138

## Appendix A

### List of the abbreviations and notations used throughout the text

AS: sequential ablation  
AZO: ZnO doped with Al  
BC/BI/BV: conduction/forbidden/valence band  
D: dopant  
DFT: density functional theory  
DRX: X-ray diffraction  
FL: photoluminescence  
FM: ferromagnetism, ferromagnetic  
 $H_c$ : coercive field  
MT: transition metal  
 $M_s$ : saturation magnetization  
 $n_e$ : electron concentration  
NZO: ZnO doped with Ni  
PLD: pulsed laser deposition  
SMD: diluted magnetic semiconductor  
SS: thin films  
 $T_c$ : Curie temperature  
 $V_O$ : oxygen vacancy  
XPS: X-ray photoelectron spectroscopy  
 $Zn_i$ : zinc interstitial

## List of papers already published or submitted for publishing

### Papers in ISI indexed journals

1. D.Mardare, N.Iftimie, M.Crişan, M.Răileanu, A.Yildiz, **T.Coman**, K.Pomoni, A. Vomvas, *Electrical conduction mechanism and gas sensing properties of Pd-doped TiO<sub>2</sub> films*, J Non-Cryst Solids 357 (2011), 1774–1779
2. V.Tiron, **T.Coman**, L.Sirghi, G.Popa, *Atomic force microscopy investigation of piezoelectric response of ZnO thin films deposited by HIPIMS*, J Optoelectron Adv M **15**(2013), 77 - 81

### Papers submitted for publishing in ISI indexed journals

**T. Coman**, C. Ursu, V. Nica, L. Ursu, M. Olaru, C. Cotofana, V. Tiron, M. Dobromir, A. Coroaba, O. G. Dragos, N. Lupu, O. F. Caltun, *Sequential laser ablation of metallic targets for Al-doped ZnO thin films deposition*, trimis spre publicare în Journal of Physics D: Applied Physics

### Works presented at scientific manifestations:

- 3 at national conferences, of which 3 poster presentations
- 5 at international conferences, of which 4 poster presentations and one invited talk